

Finite Element Modeling of Woodwind Instruments

Antoine Lefebvre and Gary P. Scavone

Computational Acoustic Modeling Laboratory (CAML)
Centre for Interdisciplinary Research in Music Media and Technology (CIRMMT)
Schulich School of Music of McGill University
555 Sherbrooke Street West, Montreal, QC H3A 1E3, Canada

PACS: 43.75.Ef,43.20.Mv

ABSTRACT

The input impedance of simple woodwind-like instruments is evaluated using the Finite Element Method (FEM) and compared to theoretical calculations based on the transmission-matrix method (TMM). Thermoviscous losses are accounted for with an impedance boundary condition based on acoustic boundary layer theory. The systems are surrounded by a spherical radiation domain with a second-order non-reflecting spherical-wave boundary condition on its outer surface.

For simple geometries, the FEM results are shown to match theory with great accuracy. When considering toneholes, boundary layer losses must be added to the TMM model to achieve good agreement with the FEM calculations. For geometries with multiple closed or open toneholes, discrepancies between the FEM and the TMM results become more significant and appear related to internal or external interactions. For closed side holes, this effect is more important at low frequencies, thus affecting the first few resonances. For open side holes, this effect is particularly important near the tonehole cutoff frequency but extends to lower frequencies as well. In general, the TMM does not model tonehole interactions, thus posing a limitation to its accuracy.

INTRODUCTION

The input impedance of woodwind instruments is typically calculated using the Transmission-Matrix Method (TMM) (Plitnik and Strong 1979; Caussé et al. 1984; Keefe 1990). The TMM approximates the geometry of a structure as a sequence of concatenated one-dimensional cylindrical or conical segments. Toneholes are considered to exist at their center point, between adjacent segments. The TMM evaluates only the acoustic field within a system. Thus, the use of the TMM to model musical instruments with complex geometries (bends, open holes, ...) will likely lead to errors of unknown magnitude. Further, one of the hypotheses on which the transmission matrix method is based – that the evanescent modes excited near each discontinuity decay sufficiently within each segment of the model to be independent from one another – is generally not fulfilled, as reported by Keefe (1983).

In this paper, we make use of the Finite Element Method (FEM) to calculate the input impedance of woodwind-like instrument geometries and compare the results with the TMM. The FEM solves the Helmholtz equation $\nabla^2 p + k^2 p = 0$, taking into account any complexities of the geometry under study with no further assumptions. There are two primary problems in using the FEM for this purpose: (1) how to properly model the boundary layer losses in the instruments; and (2) how to model the sound radiation into a free field. We present solutions to these problems and show that the FEM provides a valuable computational approach for woodwind instrument modeling, both for the verification of the accuracy of the TMM and for handling complex geometries. The main disadvantage of the FEM compared to the TMM is the excessively long calculation time (hours instead of seconds).

The results reported in this paper focus primarily on compar-

isons of resonance frequency values as determined using the FEM and TMM. Where appropriate, we also calculate variations in computed values in cents. There are 100 cents in an equal-tempered semitone and the interval in cents between two frequencies f_1 and f_2 is determined as $1200 \log_2(f_2/f_1)$. It has been reported by Helmholtz (1945, Sec. G) that adjustments by players of up to ± 20 cents from equal tempered tuning are required in certain musical contexts. Thus, we feel that a musical instrument should be designed with a tuning precision of ± 1 cent with respect to an equal tempered scale, with a maximum limit of ± 5 cents deviation, in order to avoid overly burdening a player with extreme tuning adjustments during performance.

In the next section, we present the details of the boundary conditions used for the FEM simulations. Then, details of the TMM equations are reviewed. Finally, the results of simulations of instrument-like systems of increasing complexity are presented.

FEM DETAILS

Our FEM simulations were computed using the software package COMSOL. All open simulated geometries include a surrounding spherical radiation domain that uses a second-order non-reflecting spherical boundary condition on its surface, as described by Bayliss et al. (1982). Further discussion on this topic can be found in Tsynkov (1998) and Givoli and Neta (2003).

Thermoviscous boundary layer losses may be approximated with a special boundary condition such as presented by Pierce (1989, p. 528), Bossart et al. (2003) or Chaigne et al. (2008, p. 211, Eq. 5.138). It is the expression from Chaigne et al. (2008) that we implemented as our boundary condition (with a

minor correction, the term $\gamma - 1$ was missing):

$$Y_{wall} = -\frac{v_n}{p} = \frac{1}{\rho c} \sqrt{jk} \left[\sin^2 \theta \sqrt{l_v} + (\gamma - 1) \sqrt{l_t} \right]. \quad (1)$$

The meaning of the mathematical symbols are:

v_n	normal velocity on the boundary,
$k = 2\pi f/c$	wave number,
θ	angle of incidence of the wave,
μ	fluid viscosity,
ρ	fluid density,
γ	ratio of specific heats,
c	speed of sound in free space,
Pr	Prandtl number,
$l_v = \mu/\rho c$	vortical characteristic length,
$l_t = l_v/Pr$	thermal characteristic length.

The angle of incidence may be calculated from $\cos \theta = \hat{n} \cdot \hat{v}/|\hat{v}|$, where the normal vector \hat{n} is unit length. The properties of air at 25°C are used for all the simulation cases.

From the simulation results, the input impedance is evaluated by dividing the complex values of the pressure and normal velocity found on the input plane. Because the solution is computed as a plane wave near the input end (which is defined at least 3 to 5 times the diameter of the pipe away from the first tonehole), these values are constant on the surface. In order to average any numerical errors, we perform an average on the surface: $p_{in} = (1/S_{in}) \int_{S_{in}} p dS$ and $v_{in} = (1/S_{in}) \int_{S_{in}} v dS$. The normalized input impedance is then $\bar{Z}_{in} = p_{in}/\rho c v_{in}$.

For all the simulation results in this paper, curved third-order Lagrange elements are used. The resonance frequencies of the simulated objects are estimated by a linear interpolation of the zeros of the angle of the reflection coefficient $R = (Z - 1)/(Z + 1)$. The simulations are performed from 100Hz to 1500Hz in steps of 10Hz.

TMM DETAILS

In the following sections, the results of FEM simulations of instruments of increasing complexities are compared to theoretical calculations using the TMM. All studied systems are comprised of cylindrical or conical bores with open or closed toneholes. The theoretical expression of the transmission matrix of a lossy cylinder is:

$$\mathbf{T}_{cyl} = \begin{bmatrix} \cosh(\Gamma L) & \bar{Z}_c \sinh(\Gamma L) \\ \sinh(\Gamma L)/\bar{Z}_c & \cosh(\Gamma L) \end{bmatrix}, \quad (2)$$

where Γ is a complex-valued propagation wavenumber and \bar{Z}_c is a complex-valued characteristic impedance. They can be calculated exactly with $\Gamma = \sqrt{\bar{Z}_v \bar{Y}_t}$ and $\bar{Z}_c = \sqrt{\bar{Z}_v/\bar{Y}_t}$, where

$$\bar{Z}_v = jk \left(1 - \frac{2}{k_v a} \frac{J_1(k_v a)}{J_0(k_v a)} \right)^{-1}, \quad (3)$$

$$\bar{Y}_t = jk \left(1 + (\gamma - 1) \frac{2}{k_t a} \frac{J_1(k_t a)}{J_0(k_t a)} \right). \quad (4)$$

The meaning of the symbols are:

a	radius of the waveguide,
$k_v = \sqrt{-jk/l_v}$	viscous diffusion wave number,
$k_t = \sqrt{-jk/l_t}$	thermal diffusion wave number,
J_0	Bessel function of order 0,
J_1	Bessel function of order 1.

Various references discuss the theory of wave propagation in a waveguide with boundary layer losses (Kirchhoff 1868; Tijdeman 1975; Keefe 1984; Pierce 1989; Chaigne et al. 2008).

The transmission matrix of a lossy conical waveguide is (Kulik 2007):

$$\mathbf{T}_{cone} = \begin{bmatrix} -rt_{out} \sin(\bar{k}L - \theta_{out}) & ir\bar{Z}_c \sin(\bar{k}L) \\ irt_{in}t_{out} \sin(\bar{k}L + \theta_{in} - \theta_{out})/\bar{Z}_c & rt_{in} \sin(\bar{k}L + \theta_{in}) \end{bmatrix}, \quad (5)$$

where x_{in} and x_{out} are respectively the distance from the apex of the cone to the input and output planes of the cone, $r = x_{out}/x_{in}$, $L = x_{out} - x_{in}$ is the length of the cone, $\theta_{in} = \arctan(kx_{in})$, $\theta_{out} = \arctan(kx_{out})$, $t_{in} = 1/\sin \theta_{in}$, $t_{out} = 1/\sin \theta_{out}$ and $\bar{k} = (1/L) \int_{x_{in}}^{x_{out}} k(x) dx$, where $k(x)$ is the propagation constant ($k = i\Gamma$ in our notation) which depends on the radius at the position x .

Two different tonehole models are compared in this paper, including that of Dalmont et al. (2002) and an updated model from Lefebvre and Scavone (2010) (which itself is derived using the FEM). The transmission matrix of the tonehole is defined as:

$$\mathbf{T}_{hole} = \begin{bmatrix} 1 + \frac{\bar{Z}_a}{2\bar{Z}_s} & \bar{Z}_a(1 + \frac{\bar{Z}_a}{4\bar{Z}_s}) \\ 1/\bar{Z}_s & 1 + \frac{\bar{Z}_a}{2\bar{Z}_s} \end{bmatrix}. \quad (6)$$

For the model of Dalmont et al. (2002):

$$\bar{Z}_s^{(o)} = j(kt_i + \tan k(t + t_m + t_r)), \quad (7)$$

$$\bar{Z}_a^{(o)} = jkt_a, \quad (8)$$

$$\bar{Z}_s^{(c)} = -j \cot k(t + t_m), \quad (9)$$

$$\bar{Z}_a^{(c)} = jkt_a, \quad (10)$$

where $t_i/b = 0.82 - 1.4\delta^2 + 0.75\delta^{2.7}$, $t_a/b = -0.28\delta^4$, $t_m/b = \delta(1 + 0.207\delta^3)/8$ and t_r is calculated with Eq. 12. When boundary layer losses are included, k is replaced by $k_c = \omega/c + (1 - j)\alpha$ with $\alpha = (1/b)\sqrt{kv/(2\rho c)}(1 + (\gamma - 1)/v)$, where $v = \sqrt{Pr}$.

For the updated tonehole model, Eqs. 35, 37 and 40 are used from Lefebvre and Scavone (2010) with a modification to the open shunt impedance to include boundary layer losses, which becomes:

$$\bar{Z}_s^{(o)} = j \tan \{kt_r + k_c(t_i + t + t_m)\}. \quad (11)$$

In the formulation by Dalmont et al. (2002), the inner length correction does not include boundary layer losses. We found a better match with the simulation results if the inner length correction, but not the radiation length correction, includes boundary layer losses.

The open end of our instrument-like systems are modeled with a semi-infinite unflanged pipe radiation impedance given by (Caussé et al. 1984):

$$\bar{Z}_r = 0.6113 jka - j(ka)^3 [0.036 - 0.034 \log ka + 0.0187(ka)^2] + (ka)^2/4 + (ka)^4 [0.0127 + 0.082 \log ka - 0.023(ka)^2]. \quad (12)$$

VALIDATION

The FEM approach was validated for geometries where the TMM is known to be accurate (for 1D wave propagation). These configurations included a cylindrical and a conical waveguide

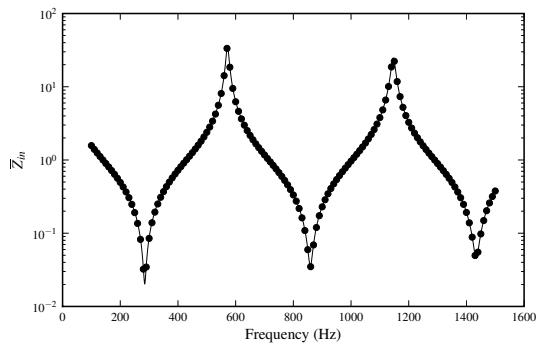


Figure 1: Normalized input impedance of a closed cylinder of diameter 15 mm and length 300 mm: FEM results (filled circles) and theoretical solution (solid line).

with varying boundary conditions at their ends. We were particularly interested in verifying the accuracy of the boundary layer impedance model and non-reflecting radiation boundary condition.

A 3D FEM simulation of a closed cylindrical pipe of diameter 15 mm and length 300 mm was first computed. To minimize computation time, system symmetries were exploited. The cylinder was split in two along its primary axis and a null normal acceleration boundary condition was imposed on the plane of symmetry. A rigid boundary ($\hat{v}_n = 0$) was created at the pipe end, while the boundary condition along the side walls was that given by Eq. 1. The results of the FEM simulation (filled circles) are shown in Fig. 1 compared to the TMM calculations (solid line). The mesh consists of 2003 cubic elements, giving a total of 12354 degrees of freedom. The first resonance frequency obtained using the FEM and TMM was 571.74 Hz and 571.69 Hz, respectively, a difference smaller than 0.2 cents. The ratio of the resonance magnitude is about 0.1 dB. Results for the second resonance were even closer, indicating that the boundary condition for wall losses provides accurate results.

The second validation simulation involved replacing the rigid boundary at the pipe output with the impedance boundary condition of Eq. 12, which is the same expression used for the TMM calculations. Discrepancies were again below 0.2 cents.

Next, we simulated the same cylindrical pipe but with the open end radiating into a spherical radiation domain of 50 cm radius and a non-reflecting boundary condition on its outer edge. The exterior of the pipe was considered rigid (boundary layer losses were neglected outside the pipe). We found that the refinement of the mesh along the edge at the opening of the pipe influences significantly the radiation length correction of the pipe. We simulated the same open pipe with an increasing number of elements on this edge and found that the circumference must be approximated with about 300 elements to attain numerical convergence. Once again, discrepancies were below 0.2 cents.

The same procedure was performed for a conical pipe of length 300 mm, with an input diameter of 15.0 mm and an output diameter of 30.7 mm (half angle is 1.5 degrees). The discrepancies between the resonance frequencies computed using the FEM and TMM were slightly larger than for the cylindrical geometry, but they were still below 0.5 cents for the closed cone and the cone terminated by the radiation impedance. We believe these discrepancies may come from the theoretical model (Kulik 2007), which does not take into account the variation of the complex characteristic impedance along the cone. This error is sufficiently small to be neglected. For the cone radiating into a

Method	f_1 [Hz] (cents)	f_2 [Hz] (cents)
Cylinder with one hole closed		
FEM	280.68	842.84
Dalmont w/o losses	280.80 (0.7)	842.90 (0.1)
Dalmont with losses	280.80 (0.7)	842.86 (0.1)
Lefebvre w/o losses	280.72 (0.3)	842.90 (0.1)
Lefebvre with losses	280.71 (0.1)	842.86 (0.1)
Cylinder with one hole open		
FEM	378.80	1123.83
Dalmont w/o losses	379.07 (1.2)	1125.18 (2.1)
Dalmont with losses	378.97 (0.8)	1124.93 (1.7)
Lefebvre w/o losses	379.01 (1.0)	1124.32 (0.7)
Lefebvre with losses	378.82 (0.1)	1123.85 (0.0)
Cone with one hole closed		
FEM	362.32	872.46
Dalmont w/o losses	362.63 (1.5)	872.84 (0.8)
Dalmont with losses	362.62 (1.4)	872.83 (0.7)
Lefebvre w/o losses	362.42 (0.5)	872.49 (0.1)
Lefebvre with losses	362.41 (0.4)	872.47 (0.0)
Cone with one hole open		
FEM	572.85	1019.35
Dalmont w/o losses	573.98 (3.4)	1020.70 (2.3)
Dalmont with losses	573.86 (3.1)	1020.55 (2.0)
Lefebvre w/o losses	573.57 (2.2)	1019.46 (0.2)
Lefebvre with losses	573.30 (1.4)	1019.11 (-0.4)

Table 1: Comparison of the resonance frequencies for the cylindrical and conical waveguide with one open or closed tonehole. The numbers in parentheses represent the intervals in cents relative to the FEM result.

sphere, the first resonance was approximately 1 cent lower in the FEM simulation, indicating that the radiation model of an unflanged pipe may be inadequate when used at the end of a conical waveguide (though the discrepancy is relatively small).

From these validation tests, we conclude that the boundary condition for the thermoviscous losses and the non-reflecting spherical wave boundary condition can be used successfully for the simulation of woodwind instruments and that the maximum error in the calculated resonance frequencies up to 1500 Hz using the TMM is on the order of 1 cent.

WAVEGUIDES WITH A SINGLE TONEHOLE

The input impedance of a cylindrical and a conical waveguide with a single tonehole was calculated with the FEM and TMM. These geometries allow us to verify the accuracy of the tonehole models while avoiding possible interactions between adjacent holes. In the FEM, the boundary condition approximating the boundary layer losses is defined on all interior surfaces, including the tonehole walls. Boundary layer losses are not normally accounted for along tonehole walls using the TMM. Thus, discrepancies between the FEM and TMM results in this section are primarily attributable to these losses and, for the conical waveguide, the influence of a main bore taper.

The cylindrical and conical pipes described in the validation section were modified to include a tonehole of height $t = 2$ mm and $\delta = b/a = 0.7$. For the cylindrical pipe, the tonehole is located at 87.7 mm from the open end, while it is located at 141.4 mm from the open end of the conical waveguide.

The FEM simulations are in good agreement with TMM calculations for closed side holes. The revised TMM model proposed in

Method	f_1 [Hz] (cents)	f_2 [Hz] (cents)	f_3 [Hz] (cents)	f_4 [Hz] (cents)
Closed toneholes				
FEM	143.23	297.43	460.45	630.03
Dalmont with losses	144.01 (9.3)	298.39 (5.6)	461.02 (2.1)	630.73 (1.9)
Lefebvre with losses	143.45 (2.5)	297.72 (1.7)	460.62 (0.6)	630.00 (-0.1)
Open toneholes				
FEM	172.26	364.93	569.13	774.87
Dalmont with losses	172.62 (3.6)	365.77 (3.9)	570.81 (5.1)	778.62 (8.4)
Lefebvre with losses	172.63 (3.8)	365.73 (3.8)	570.48 (4.1)	777.26 (5.3)

Table 2: Comparison of the simulated and calculated resonance frequencies of a conical waveguide with three open or closed toneholes.

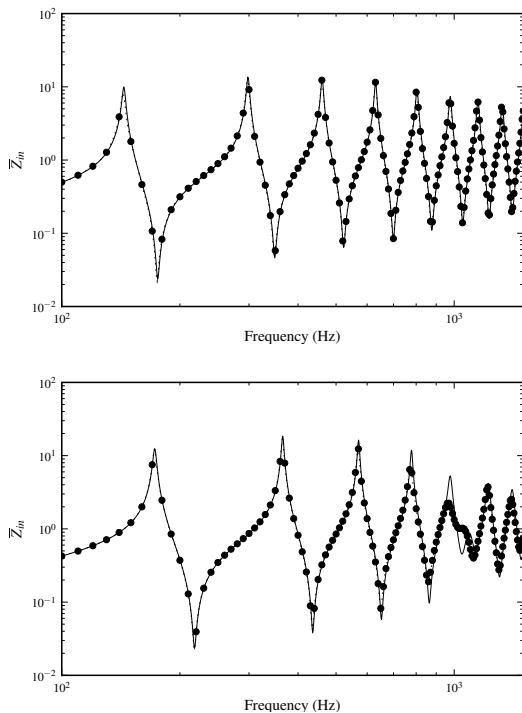


Figure 2: Input impedance of a conical waveguide with three toneholes: all closed (top graph) and all open (bottom graph). Comparison between the FEM (filled circles) and the TMM (solid). The dashed line is an interpolation between the FEM data points.

Lefebvre and Scavone (2010) significantly improves the results for toneholes of large diameter and short height. The incorporation of wall losses in the tonehole model does not change the resonances in this case, possibly because these toneholes are short ($t = 2$ mm). For the conical waveguide, the error of 0.4 cents for the first resonance is of the same magnitude as the error found for the conical waveguide with no toneholes in the previous section and is therefore not caused by the tonehole model.

For the open tonehole on a cylindrical bore, the updated TMM tonehole model with boundary layer losses accurately reproduces the resonance frequencies obtained with the FEM. The inner length correction needs to include boundary layer losses as in Eq. 11 to obtain a good match. The effect of the boundary layer losses on the tonehole model is expected to be more important for tall toneholes.

There is a discrepancy of 1.4 cents between the FEM and the revised open tonehole TMM model with boundary layer losses

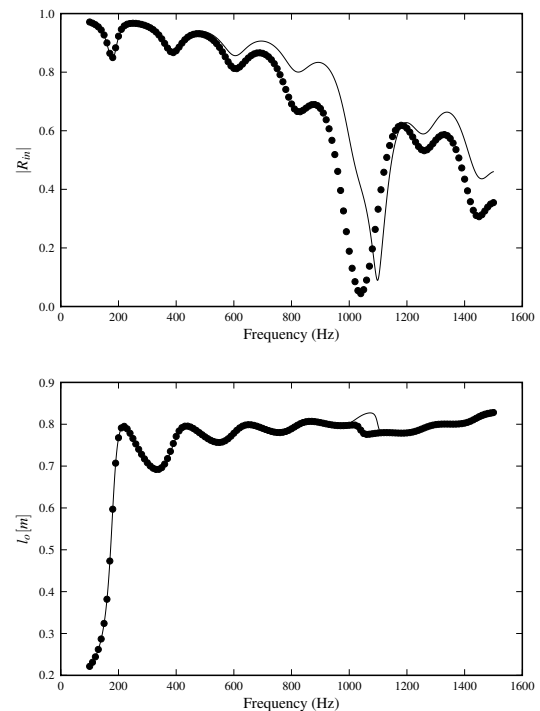


Figure 3: Magnitude of the reflection coefficient (top graph) and open cylinder equivalent length (bottom graph) for a conical waveguide with three open toneholes. Comparison between the FEM (filled circles) and the TMM (solid).

on a conical waveguide. This suggests a potential small effect of the conical waveguide taper on the behaviour of the tonehole.

A CONE WITH THREE TONEHOLES

A conical waveguide of 966.5 mm length with an input diameter of 12.5 mm and an output diameter of 63.1 mm was simulated. Three toneholes, each of 2 mm height, were located at distances of 760 mm, 818 mm and 879 mm from the input plane with respective diameters of 37.1 mm, 39.3 mm and 41.6 mm. These dimensions are close to those of the three toneholes closest to the bell of an alto saxophone. The input impedance of this instrument for all toneholes closed and all toneholes open is shown in Fig. 2.

The frequencies of the first four resonances of this system for both closed and open toneholes are presented in Table 2. When all toneholes are closed, the resonance frequencies calculated using the TMM with the Lefebvre tonehole model are significantly closer to those found using the FEM. The discrepancies between these results decrease with increasing frequency and are perhaps caused by internal tonehole interactions.

Method	f_1 [Hz] (cents)	f_2 [Hz] (cents)	f_3 [Hz] (cents)	f_4 [Hz] (cents)
Closed toneholes				
FEM	146.83	439.72	737.72	1032.82
Dalmont with losses	146.79 (-0.5)	439.74 (0.1)	737.70 (-0.1)	1032.80 (-0.1)
Lefebvre with losses	146.80 (-0.4)	439.78 (0.2)	737.77 (0.1)	1032.92 (0.2)
Open toneholes				
FEM	294.55	879.06	1448.49	
Dalmont with losses	293.44 (-6.6)	879.82 (1.5)	1452.50 (4.8)	
Lefebvre with losses	293.44 (-6.6)	879.75 (1.3)	1450.66 (2.6)	

Table 3: Comparison of the simulated and calculated resonance frequencies of a simple clarinet-like system with twelve open or closed toneholes.

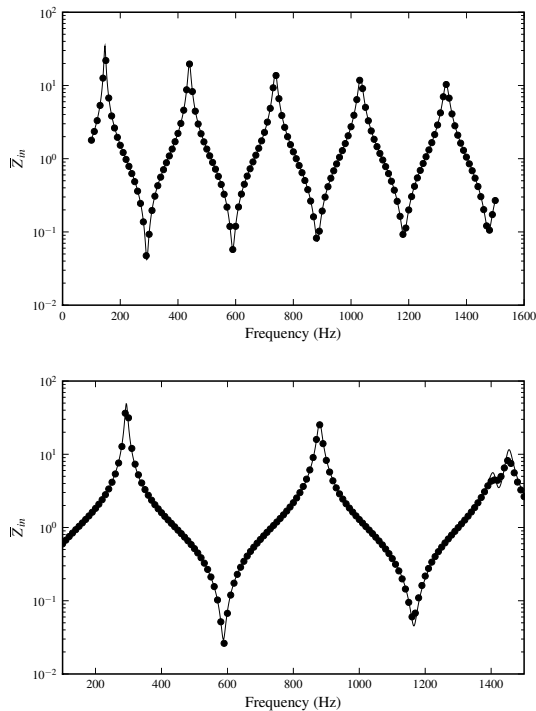


Figure 4: Input impedance of a cylindrical waveguide with 12 toneholes: all closed (top graph) and all open (bottom graph). Comparison between FEM simulation of the complete instrument (filled circles) and TMM calculations (solid).

When all toneholes are open, both TMM tonehole models predict resonance frequency values above those found using the FEM, with discrepancies increasing with frequency. Observation of the calculated input impedances in Fig. 2, as well as the reflection coefficient magnitudes and equivalent lengths in Fig. 3, indicate significant discrepancies between the FEM and TMM results near the tonehole cutoff frequency. The equivalent length is calculated as $L_o = (\pi - \phi_R)/2k$ (Ayers 1995), where ϕ_R is the unwrapped phase of the reflection coefficient. The differences are likely more attributable to internal or external tonehole interactions than to the main bore taper. In general, the FEM simulations predict lower resonance frequencies, as well as lower reflection coefficient magnitudes, which suggest that the tonehole interactions increase the amount of radiated energy. Research on how the TMM may be extended to include this effect would be necessary to further improve the TMM results.

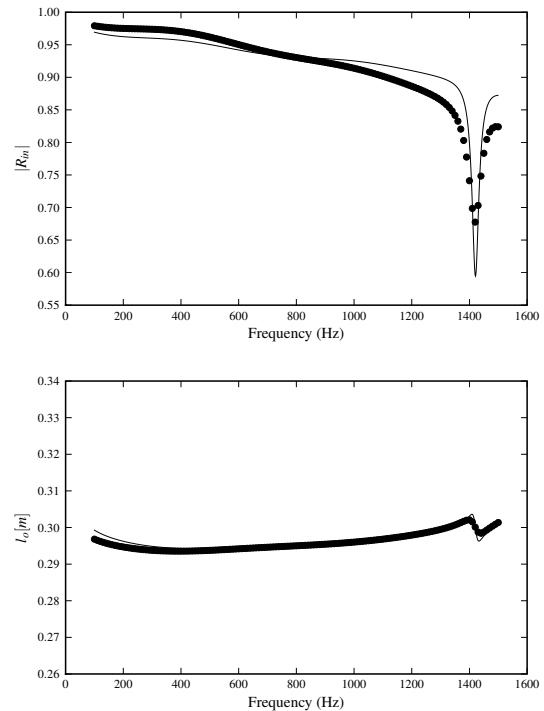


Figure 5: Magnitude of the reflection coefficient for a cylindrical waveguide with twelve open toneholes. Comparison between FEM simulation of the complete instrument (filled circles) and TMM calculations (solid).

A CYLINDER WITH TWELVE TONEHOLES

A clarinet-like system was simulated consisting of a cylindrical pipe of 15.0mm diameter and 572.2mm length with 12 toneholes of 6 mm diameter and 6 mm height located at the following distances from the instrument excitation point (in mm): 265.8, 282.6, 300.3, 319.1, 338.9, 359.9, 382.1, 405.6, 430.4, 456.7, 484.5, 514.0. These toneholes produce a one-octave chromatic scale starting at 146.8Hz (D3).

This instrument was simulated with all toneholes closed and all toneholes opened. The mesh consisted of 24863 cubic elements (125593 dof). The impedances calculated with the FEM and TMM are shown in Fig. 4. The frequencies of the resonances are compared in Table 3.

When all toneholes are closed, the TMM calculations with both tonehole models produce resonance frequencies that well match those found using the FEM, with the exception of a small difference for the first resonance. When all the toneholes

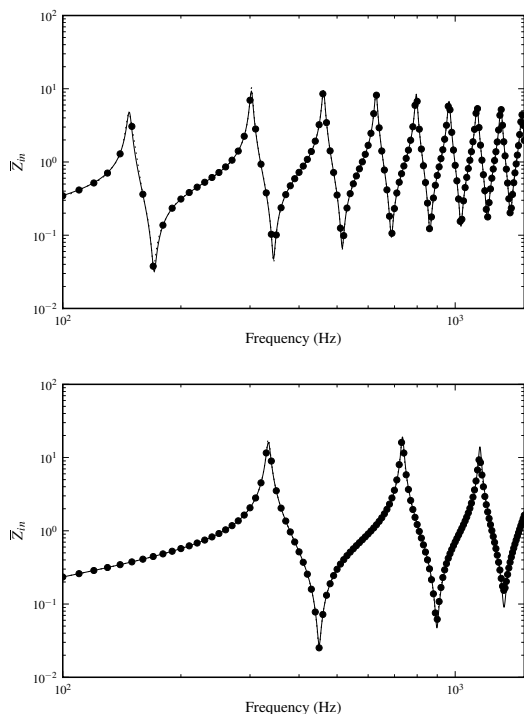


Figure 6: Input impedance of a conical waveguide with twelve toneholes: all closed (top graph) and all open (bottom graph). Comparison between FEM simulation (filled circles) and TMM calculations (solid). The dashed line is an interpolation between the FEM data points.

are open, discrepancies are more significant and are likely due to tonehole interactions. Figures 4 and 5 indicate a variation between the FEM and TMM results near the tonehole lattice cutoff frequency, which occurs at the minimum of the reflection coefficient magnitude. This again suggests that the interaction between the sound field of adjacent toneholes can shift the resonance frequencies. In this case, however, the resonance frequencies predicted by the FEM are higher than those found using the TMM.

A CONE WITH TWELVE TONEHOLES

A saxophone-like system was simulated consisting of a conical waveguide of 9 mm input diameter, 61.2 mm output diameter, and 978.9 mm length with 12 toneholes of 2 mm height located respectively at 363.6, 401.9, 441.9, 483.7, 527.4, 573.1, 620.9, 671.0, 723.7, 779.1, 837.5 and 899.1 millimeters from the input end. These toneholes, defined by $\delta = b/a = 0.7$, produce a one-octave chromatic scale starting at 146.8 Hz (D3).

The FEM simulation of this instrument was solved for all toneholes closed and all toneholes opened. The mesh consisted of 32655 cubic elements (165626 dof). The input impedances calculated with the TMM and FEM are plotted in Fig. 6 and the resonance frequency values compared in Table 4.

For the closed side holes, the TMM results using the Dalmont tonehole model differ significantly from the FEM predictions (22 cents for the first resonance and close to 10 cents for the others). Although the TMM results are closer using the Lefebvre tonehole model, discrepancies remain, particularly for the first resonance (8 cents), and support the hypothesis that internal tonehole interactions lower the low-frequency resonances when the toneholes are closed.

When the toneholes are open, the FEM predicts lower reso-

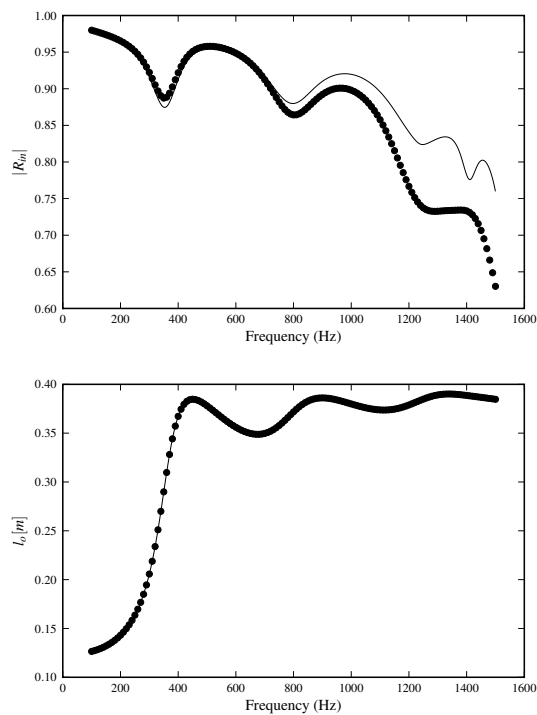


Figure 7: Magnitude of the reflection coefficient for a conical waveguide with twelve open toneholes. Comparison between FEM simulation (filled circles) and TMM calculations (solid).

nances than either of the TMM tonehole models. Again, this seems to be related to tonehole interactions. In this case, the tonehole cutoff frequency is above 1.5 kHz and the first resonance is only affected by about 1 cent, whereas the third resonance is shifted by 4 cents. Contrary to the case for the cylindrical instrument, the first resonance is not significantly affected.

CURVATURE OF THE BORE

Many wind instruments are bent for practical reasons and the question of the effect of the curvature on the acoustic properties of waveguides has captured the attention of many researchers. Rayleigh (1945) concluded that a curved tube is equivalent to a straight tube of the same length, as measured along the centre line, because the velocity potential is constant on any section perpendicular to the main axis. C. Nederveen (1998) assumed that the pressure is constant over the same cross-sections and concluded that the bent tube appears slightly shorter and wider (see p. 60), which leads to the apparent phase velocity $c\sqrt{\rho/\rho_B}$, where $\rho/\rho_B = (R^2 - R\sqrt{R^2 - a^2})/(0.5a^2)$ and R is the radius of curvature of the centre line of the tube. As reported by Brindley (1973), neither of the two assumptions can be true. Furthermore, such expressions do not consider boundary layer losses.

Many attempts at estimating the effect of curvature have been reported (Keefe and Benade 1983; C. J. Nederveen 1998; Kim and Ih 1999; Kantartzis et al. 2004; Félix et al. 2008). The influence of curvature is shown to be frequency dependant and much more complex than what simplified theories can predict. The situation becomes even more complex if the curved bore is not cylindrical and if boundary layer losses are to be taken into account.

Using the FEM and the thermoviscous boundary condition presented in this paper, the simulation of a curved bore with a varying cross-section and with boundary layer losses is pos-

Method	f_1 [Hz] (cents)	f_2 [Hz] (cents)	f_3 [Hz] (cents)	f_4 [Hz] (cents)
Closed toneholes				
FEM	147.19	302.58	461.63	628.60
Dalmont with losses	149.06 (21.9)	304.10 (8.7)	463.98 (8.8)	631.94 (9.2)
Lefebvre with losses	147.85 (7.8)	302.63 (0.3)	461.97 (1.3)	628.76 (0.2)
Open toneholes				
FEM	334.14	733.03	1154.32	
Dalmont with losses	334.31 (0.8)	734.35 (3.1)	1158.30 (6.0)	
Lefebvre with losses	334.28 (0.7)	734.06 (2.4)	1156.56 (3.4)	

Table 4: Comparison of the simulated and calculated resonance frequencies of a conical waveguide with twelve open or closed toneholes.

Method	f_1 [Hz] (cents)	f_2 [Hz] (cents)	f_3 [Hz] (cents)	f_4 [Hz] (cents)	f_5 [Hz] (cents)
straight (1)	145.03	304.92	473.41	640.97	804.22
curved (2)	145.04 (0.1)	304.97 (0.2)	473.58 (0.6)	641.30 (0.9)	804.57 (0.8)
curved (3)	145.05 (0.2)	305.09 (0.9)	473.98 (2.1)	642.07 (3.0)	805.39 (2.5)
straight (TMM)	144.90 (-1.6)	305.24 (1.8)	473.68 (1.0)	640.95 (0.0)	804.19 (-0.1)

Table 5: Comparison of the simulated and calculated resonance frequencies of a conical waveguide with twelve open or closed toneholes.

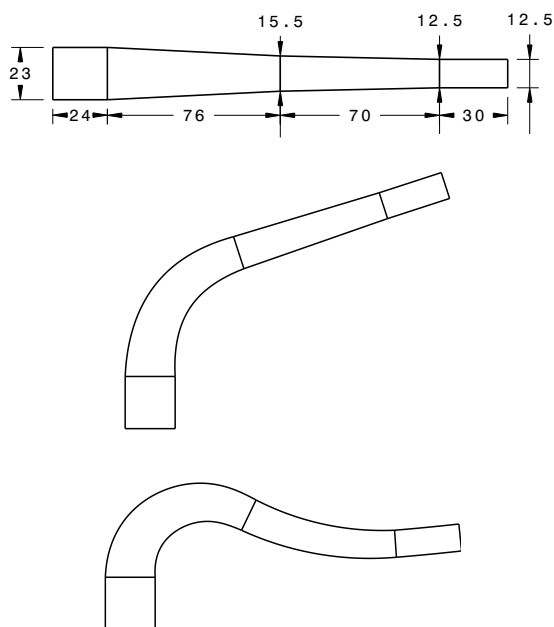


Figure 8: Diagram of the three instrument bores simulated for the study of curvature. The dimensions, in mm, are the same for all three instruments.

sible. As a case study, we present the results of simulations of a conical waveguide with different geometrical settings: (1) straight, (2) slight curvature and (3) stronger curvature, as illustrated in Fig. 8. Each of these three geometries has the same cross-sectional diameter as a function of the distance along the centre line. Therefore, they also have the same volume. Concatenated to these segments was a straight conical waveguide of 760 mm length, input diameter of 23 mm (corresponding to the output diameter of the first segment) and output diameter of 63 mm. An unflanged pipe radiation impedance was applied at the output of the conical section. From the results of the simulations, we compared the first five resonance frequencies of the curved bores to those of the straight bore. We also compared the FEM results of the straight bore with TMM calculations. These results are presented in Table 5.

The shift of resonance frequencies with bending is relatively small for the lowest resonances but gradually increases up to 3 cents for the fourth resonance of the third geometry. As expected, the object with the most significant curvature has a more pronounced frequency shift. On wind instruments, the curvature of the bore normally comes with an “ovalisation” of the section and possibly a small reduction of the volume due to the mechanical consequence of bending the tube. This effect is not discussed here and may have more pronounced consequences on the tuning.

We compared the resonance frequencies for the straight geometry with predictions of the TMM and found surprising differences (see Table 5, last line). One hypothesis is that the evanescent modes occurring when the angle of conicity changes (there are three such changes in the current geometry) are the cause of such differences.

CONCLUDING REMARKS

The resonance frequencies of woodwind instruments may be accurately estimated using the FEM with appropriate boundary conditions to account for boundary layer losses and to simulate a non-reflecting radiation domain. We expect that the FEM can be used for the design of woodwind instruments, allowing for the calculation of tuning effects caused by geometry modifications (such as adding a new tonehole).

We found that the calculation of the resonance frequencies of woodwind-like instruments using the TMM may result in errors of up to 10 cents, most likely due to mutual interactions between toneholes and the lack of boundary layer loss modeling within the TMM tonehole model. The discrepancies appear to be more important at lower frequencies in the case of closed side holes but more significant at higher frequencies in the case of open side holes. The input impedance of an instrument with many open toneholes is not well predicted by the TMM near the tonehole cutoff frequency. More research is necessary to develop a model that captures this phenomenon accurately.

ACKNOWLEDGMENTS

The authors wish to acknowledge the support of the Natural Sciences and Engineering Research Council of Canada, the Canadian Foundation for Innovation, and the Centre for Interdisciplinary Research in Music Media and Technology at

McGill University. The first author gratefully acknowledges the Fonds Québécois de la Recherche sur la Nature et les Technologies for a doctoral research scholarship.

REFERENCES

- Ayers, R. Dean (1995). "Two complex effective lengths for musical wind instruments". *J. Acoust. Soc. Am.* 98, pp. 81–87.
- Bayliss, Alvin et al. (1982). "Boundary Conditions for the Numerical Solution of Elliptic Equations in Exterior Regions". *SIAM Journal on Applied Mathematics* 42, pp. 430–451.
- Bossart, R. et al. (2003). "Hybrid numerical and analytical solutions for acoustic boundary problems in thermo-viscous fluids". *J. Sound Vibrat.* 263, pp. 69–84.
- Brindley, G. S. (1973). "Speed of Sound in Bent Tubes and the Design of Wind Instruments". *Nature* 246, pp. 479–480.
- Caussé, René et al. (1984). "Input impedance of brass musical instruments – Comparison between experimental and numerical models". *J. Acoust. Soc. Am.* 75, pp. 241–254.
- Chaigne, Antoine et al. (2008). *Acoustique des instruments de musique*. Paris, France: Éditions Belin.
- Dalmont, Jean-Pierre et al. (2002). "Experimental Determination of the Equivalent Circuit of an Open Side Hole: Linear and Non Linear Behaviour". *Acustica* 88, pp. 567–575.
- Félix, Simon et al. (2008). "Effect of bending portions of the air column on the acoustical properties of a wind instrument". *J. Acoust. Soc. Am.* 123, p. 3447.
- Givoli, Dan and Beny Neta (2003). "High-order non-reflecting boundary scheme for time-dependent waves". *Journal of Computational Physics* 186, pp. 24–46.
- Helmholtz, Hermann von (1945). *On the sensation of tone*. Dover Publications.
- Kantartzis, Nikolaos V. et al. (2004). "A 3D multimodal FDTD algorithm for electromagnetic and acoustic propagation in curved waveguides and bent ducts of varying cross". *COMPEL* 23, pp. 613–624.
- Keefe, Douglas H. (1983). "Acoustic streaming, dimensional analysis of nonlinearities, and tone hole mutual interactions in woodwinds". *J. Acoust. Soc. Am.* 73, pp. 1804–1820.
- (1984). "Acoustical wave propagation in cylindrical ducts: Transmission line parameter approximations for isothermal and nonisothermal boundary conditions". *J. Acoust. Soc. Am.* 75, pp. 58–62.
- (1990). "Woodwind air column models". *J. Acoust. Soc. Am.* 88, pp. 35–51.
- Keefe, Douglas H. and Arthur H. Benade (1983). "Wave propagation in strongly curved ducts". *J. Acoust. Soc. Am.* 74, pp. 320–332.
- Kim, Jun-Tai and Jeong-Guon Ih (1999). "Transfer matrix of curved duct bends and sound attenuation in curved expansion chambers". *Appl. Acoust.* 56, pp. 297–309.
- Kirchhoff, G. (1868). "On the Influence of Heat Conduction in a Gas on Sound Propagation". *Ann. Phys. Chem.* 134, pp. 177–193.
- Kulik, Yakov (2007). "Transfer matrix of conical waveguides with any geometric parameters for increased precision in computer modeling". *J. Acoust. Soc. Am.* 122, EL179–EL184.
- Lefebvre, Antoine and Gary P. Scavone (2010). "Refinements to the Model of a Single Woodwind Instrument Tonehole". *Proceedings of the 2010 International Symposium on Musical Acoustics*. Sydney and Katoomba, Australia.
- Nederveen, Cornelis Johannes (1998). *Acoustical Aspects of Woodwind Instruments*. Revised. DeKalb, Illinois: Northern Illinois University Press, p. 147.
- Nederveen, Cornelis Johannes (1998). "Influence of a toroidal bend on wind instrument tuning". *J. Acoust. Soc. Am.* 104, pp. 1616–1626.
- Pierce, Allan D. (1989). *Acoustics, An Introduction to Its Physical Principles and Applications*. Woodbury, New-York: Acoustical Society of America, p. 678.
- Plitnik, George R. and William J. Strong (1979). "Numerical method for calculating input impedances of the oboe". *J. Acoust. Soc. Am.* 65, pp. 816–825.
- Rayleigh, J.W.S. (1945). *The Theory of Sound*. Vol. 2. New York: Dover Publications.
- Tijdeman, H. (1975). "On the propagation of sound waves in cylindrical tubes". *J. Sound Vibrat.* 39, pp. 1–33.
- Tsynkov, S. V. (1998). "Numerical solution of problems on unbounded domains. A review". *Applied Numerical Mathematics* 27, pp. 465–532.